This is a post-referee draft, the final version is available at

https://doi.org/10.1016/j.scriptamat.2022.115169

Metastable to Stable Phase Transformation in Atmospheric Plasma Sprayed Yb-silicate Coating during Post-Heat Treatment

Emine Bakan[a]*, Yoo Jung Sohn[a], Robert Vaßen[a]

[a]Forschungszentrum Jülich GmbH, Institute of Energy and Climate Research, Materials Synthesis and Processing (IEK-1), 52425 Jülich, Germany

*Corresponding Author. Forschungszentrum Jülich GmbH, Institute of Energy and Climate Research, Materials Synthesis and Processing (IEK-1), 52425 Jülich, Germany. Tel: +49 2461 61 2785; Fax: +49 2461 61 2455, e-mail: e.bakan@fz-juelich.de.

Abstract

Yb-silicate is used as volatilization barrier material in environmental barrier coating applications. In this study, metastable to stable phase transformation in highly amorphous atmospheric plasma sprayed Yb-silicate coating was investigated during post-heat treatment. High-temperature X-ray diffraction (HT-XRD) was used to analyze the phase composition of the coating at elevated temperatures. Three metastable phases ($Yb_2Si_2O_7$ (*P*-1), Yb_2SiO_5 ($P2_1/c$), $Yb_{4.67}Si_3O_{13}$ ($P6_3/m$)) and two stable phases ($Yb_2Si_2O_7$ (*C*2/*m*), Yb_2SiO_5 (*I*2/*a*)) preferentially crystallized from the amorphous coating starting at 1000 °C. Metastable phases transformed into stable $Yb_2Si_2O_7$ and Yb_2SiO_5 at higher temperatures. HT-XRD data were used to estimate the volume expansion in the coating due to the phase transformation and the results were compared to the dilatometry measurements. The estimated expansion from HT-XRD data was larger than the measured expansion in dilatometry. Microstructural investigation revealed crack healing in the coating during the measurements which was associated with the lower expansion measured in dilatometry.

Keywords: Environmental barrier coating, plasma spray, phase transformation, crystallization, crack healing

SiC fiber-reinforced SiC matrix ceramic matrix composites (SiC/SiC CMCs) are advanced structural materials to be used in hot sections of advanced gas turbine engines. These materials have a higher temperature capability than Ni-based superalloys, which can reduce cooling air requirements and provide an increased thrust-to-weight ratio. These benefits have led to SiC/SiC CMCs to be considered as key elements for more efficient and environmentally friendly propulsion and energy generation systems [1-5]. For protecting the SiC-based CMCs from the water vapor atmosphere in the engine, Environmental Barrier Coatings (EBCs) are being developed [6-13]. In water vapor-containing environments, silica (SiO_2) formation on SiC is accelerated [14, 15], and furthermore, SiO_2 is not stable and forms $Si(OH)_4(g)$ [16, 17]. The latter results in severe SiC recession during long-term, high-temperature, high-pressure, and high-velocity water exposures [18-20]. For that reason, unlike the porous thermal barrier coatings (TBCs) that are used to increase the temperature capability of Ni-based superalloys, EBCs are required to be dense to prevent the access of water vapor to the SiC or Si bond coat interface. Currently, typical EBC systems consist of a Si bond coat as an oxidation barrier as well as a volatilization barrier made of rare earth silicates such as $Yb_2Si_2O_7$.

Deposition of glass-forming $Yb_2Si_2O_7$ by the well-established atmospheric plasma spray (APS) method is proven to be challenging due to high cooling rates in the process and preferential

volatilization of SiO_2 from the molten particles resulting in highly amorphous deposits in the as-sprayed state with secondary phases such as Yb_2SiO_5 [8, 10, 21, 22]. Furthermore, crystallization of metastable Yb_2SiO_5 and $Yb_2Si_2O_7$ was shown at elevated temperatures (1000 °C-1200 °C) along with the stable forms of the same stoichiometries as summarized in Table 1 [23]. Garcia et al. reported that $Yb_2Si_2O_7$ (M=metastable) and Yb_2SiO_5 (M) transform into $Yb_2Si_2O_7$ (S=stable) and Yb_2SiO_5 (S) respectively at about 1200 °C. These M →S transformations were associated with a rapid linear expansion in the coating (~2 % at ~1200 °C, detected by the dilatometry measurements) due to the lower density of stable phases than that of the metastable forms. However, Garcia et al. also argued that M→S phase transformations alone may have not accounted for all the linear expansion observed in their study [23]. It was suggested that the increase in the porosity caused by the generation of thin inter-splat pores upon heat exposure significantly contributed to the overall expansion in the coating during the dilatometry measurements. However, at what temperature and why porosity increased or how it contributed to the expansion at 1200 °C remained unknown in Garcia´s study.

Table 1: Stable and metastable phases detected in the APS coating deposited from $Yb_2Si_2O_7$ feedstock at elevated temperatures [23].

Composition	Metastable (M) /Stable (S)	Crystal structure & Space Group	Temperature range (°C)
$Yb_2Si_2O_7$	M	Triclinic, *P*-1	1000-1200
Yb_2SiO_5	M	Monoclinic, $P2_1/c$	1000-1200
$Yb_2Si_2O_7$	S	Monoclinic, *C*2/*m*	1000-1300
Yb_2SiO_5	S	Monoclinic, *I*2/*a*	1000-1300

Aiming for a better understanding of the phase transformations in the amorphous APS Yb-silicate coating during the heat exposure and the resultant expansion, a free-standing APS coating was analyzed by high-temperature X-ray diffraction (HT-XRD) and dilatometry methods in this study. The coating was manufactured by using a commercial $Yb_2Si_2O_7$ feedstock (15-65 µm, Oerlikon Metco US Inc., Westbury, New York, USA) in a MultiCoat system (Oerlikon Metco, Wohlen, Switzerland) with a three-cathode TriplexPro 210 spray torch mounted on a six-axis robot (IRB 2400, ABB, Switzerland). Plasma spray conditions are summarized in Table 2. A ~2 mm thick coating was deposited on a graphite substrate and subsequently, the substrate was mechanically removed to obtain a free-standing coating. The coating was cut into $25 \times 2 \times 3$ mm^3 bar samples for dilatometry measurements and $10 \times 10 \times 2$ mm^3 samples for HT-XRD. The dilatometry measurements were conducted in air with a Netzsch DIL 402C dilatometer (Netzsch GmbH, Selb, Germany) using a heating rate of 10 K/min. 0.25 N force was applied to the samples by the push road during the measurements. HT-XRD was performed using the Empyrean diffractometer (Malvern Panalytical GmbH, Almelo, Netherlands) which was set up with Cu K α source and Bragg-Brentano geometry combined with primary and secondary fixed divergence and soller slits. The measurements were performed in air using 10 K/min heating rate, between 10-80° 2theta and each measurement took approximately 31 min. An environmental heating chamber HTK1200N (Anton Paar GmbH, Graz, Austria), which allows a homogenous temperature distribution during the data collection, was used for the HT-XRD measurements. Quantitative phase analysis of XRD patterns was performed using Rietveld Analysis [24] (TOPAS V4 Software, Bruker AXS GmbH, Karlsruhe, Germany). The microstructure of the as-sprayed samples and the samples after the dilatometry measurements were examined by scanning electron microscopy (SEM, ULTRA 55, Carl Zeiss NTS GmbH, Oberkochen, Germany) in the backscattered electron (BSE) mode and EDS (Octane Puls, EDAX, Ametek GmbH, Meerbusch, Germany).

Table 2: Summary of APS deposition parameters.

Plasma gas composition (standard liter per minute)	Power (kW)	Robot velocity (mm/s)	Stand-off distance (mm)
49Ar/1H_2	40.3	500	90

Fig. 1a shows the HT-XRD measurement results of the APS Yb-silicate between 900 °C-1200 °C. At 900-950 °C, the coating was still largely amorphous as in the as-sprayed state. Starting at 1000 °C, particularly at the second scan, crystallization into metastable and stable phases started. At 1050-1100 °C, the crystallization was largely completed but not fully as the amorphous humps were still visible in the background. At 1150 °C, the transformation into stable $Yb_2Si_2O_7$ and Yb_2SiO_5 was completed. At the second scan at 1150 °C and later at 1200 °C, the intensity of $Yb_2Si_2O_7$ and Yb_2SiO_5 peaks grew and along with that the background was flattened suggesting no amorphous content anymore. In order to slow down and analyze the M→S phase transformation at 1150 °C, a second HT-XRD measurement was performed at 1100 °C for about 20 h as shown in Fig. 1b. For this experiment, the as-sprayed sample was directly heated to 1100 °C, and the measurements were started after 2 min reaching 1100 °C. Within the first ~8 h at 1100 °C, the metastable phases were largely transformed into stable $Yb_2Si_2O_7$ and Yb_2SiO_5. In the next 7-8 h, the peak intensities of the stable phases increased while metastable phases completely diminished. In the last several hours of measurements, no changes were detected in the peak profiles and thus the measurement was stopped.

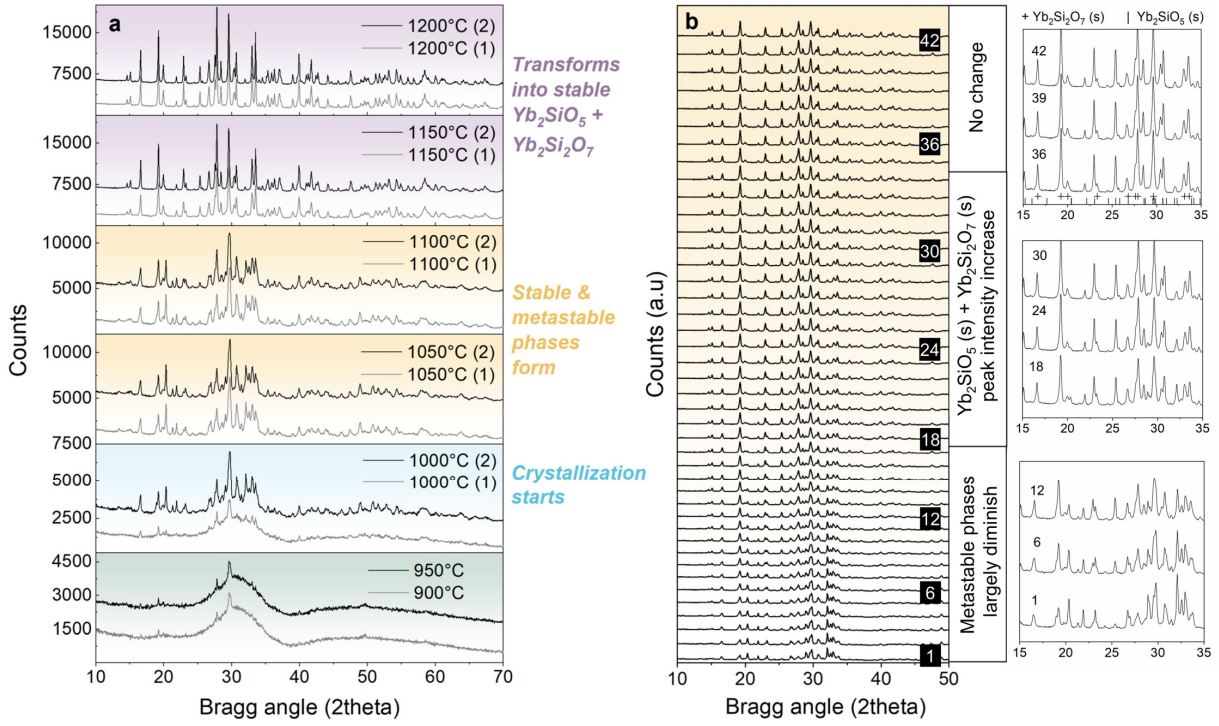

Fig. 1: HT-XRD measurement results of APS Yb-silicate coating between 900-1200 °C (a) and at 1100 °C (b). In (a), (1), and (2) after the measurement temperatures indicate the number of scans made at the given temperature. In (b), 1-42 indicate the number of the scans measured at 1100 °C, and detailed views of selected diffractograms are shown at right. Note that each scan takes about 31 min.

The phase analysis result of the 1st measurement made at 1100 °C is presented in Fig. 2. Degree of crystallinity (100 x (crystalline content / (crystalline + amorphous content)) from this first scan was estimated as 96 % which increased up to 99 % after the last scan (42nd~20 h). Crystalline and amorphous contents in the formula are equal to integral intensities of crystalline peaks and amorphous humps (around 2theta ~30° and 50°), respectively. In total five different phases (2 stable and 3 metastable) were identified at this temperature. ICSD numbers of each phase used for the Rietveld analysis can be found in the supplementary data. In addition to two metastable phases reported also in [23], Yb-silicate oxy-apatite ($Yb_{4.67}Si_3O_{13}$, $P6_3/m$) was detected in the coating as a third metastable phase. The Yb-apatite peak list (see supplementary file) was generated through the software TOPAS, according to the Rietveld analysis performed on the 1100 °C XRD data shown in Fig. 2. $Y_{4.67}Si_3O_{13}$ (ICSD No. 258724) was chosen as a starting model for the Rietveld refinement and by replacing all Y atom positions (6*h*- and 4*f*-Wyckoff positions) with Yb, peak positions and intensities for $Yb_{4.67}Si_3O_{13}$ were calculated. In terms of silica content ($7Yb_2O_3.9SiO_2$), the apatite falls in between Yb_2SiO_5 and $Yb_2Si_2O_7$ phases. The formation of metastable apatite together with the metastable $Yb_2Si_2O_7$ and Yb_2SiO_5 as observed in this work was reported by Felsche when the $7Yb_2O_3.9SiO_2$ powder mixture was heated above 1000 °C [25]. Furthermore, the metastable Y-apatite phase was also detected starting at ~1000 °C in Y-silicate coatings deposited from the vapor phase in the literature [26, 27].

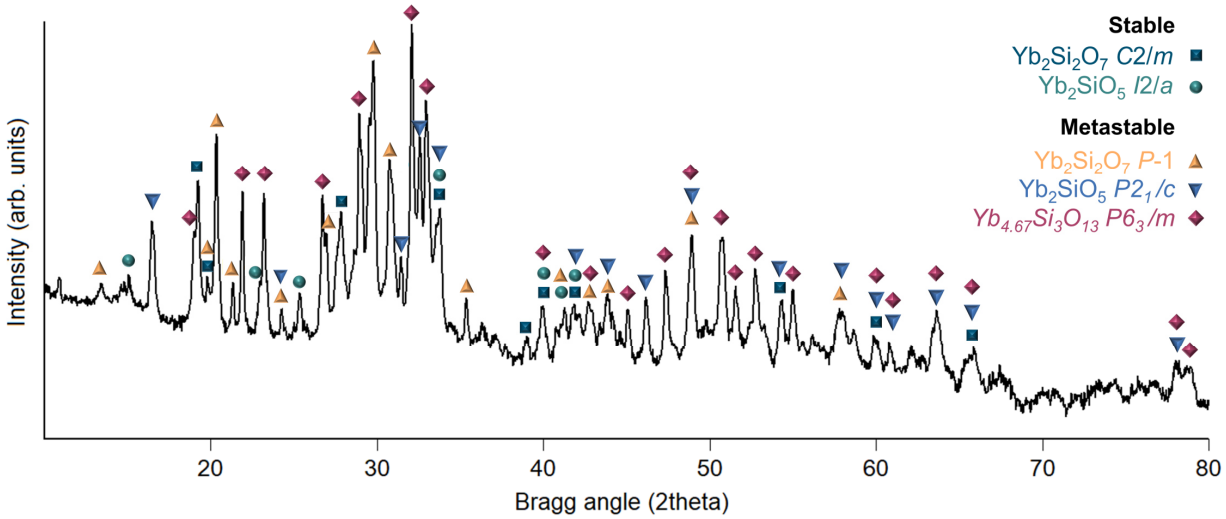

Fig. 2: Phase analysis of the 1st scan measured at 1100 °C shows the presence of metastable and stable phases as well as amorphous content. Major peaks were marked with the assigned symbols for each phase, more than one symbol for a single peak indicates overlapping of peak positions.

The quantitative phase analysis results of all scans collected at 1100 °C are shown in Fig. 3a. As the density of the amorphous phase could not be verified without knowing its stoichiometry, the coating was assumed to be 100 % crystalline for the quantitative phase analyses and hence for the volume expansion calculations. The weighted R-factor (R_{wp}) of the analysis with this

assumption was 5.41. According to Fig. 3a, at the beginning of the measurement, the coating consisted of ~75 wt.% metastable phases which transformed into stable $Yb_2Si_2O_7$ and Yb_2SiO_5 during the measurements. These results suggested that metastable Yb-silicate oxy-apatite separated into $Yb_2Si_2O_7$ and Yb_2SiO_5 phases as no other stable phases were detected. The coating contained ~40 wt.% Yb_2SiO_5 (S) phase at the end of the measurement (Fig. 3a). This high secondary phase content can be explained by the high plasma enthalpy used in the deposition process which was intentionally chosen to achieve high amorphous content and hence a high volume of metastable phases to ease the detection in XRD. Fig. 3b shows the theoretical densities of the five detected phases at 1100 °C. Lattice parameters for each phase were determined from the recorded XRD pattern at this temperature and used for theoretical density calculations. Using the weight percentages of the phases and their densities, the volume expansion of the coating ($\Delta V/V_0=(V-V_0)/V_0$) at 1100 °C was estimated assuming the initial coating volume (V_0) to be the volume of the coating determined after the 1st scan which takes about 30 min ($V_0=V_{30\ min}$). Finally, 1/3 of the volume expansion was approximated as the linear expansion, and accordingly, ~1.8 % expansion was calculated in the coating as a result of M→S phase transformation at 1100 °C (Fig.3c).

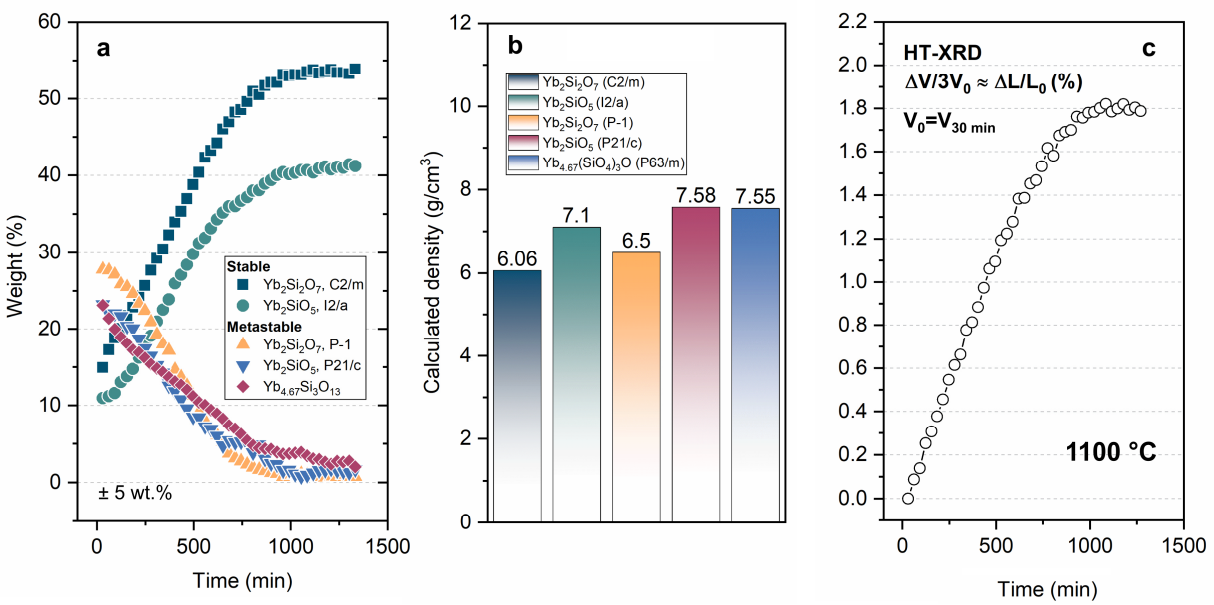

Fig. 3: The quantitative phase analysis results at 1100 °C (a), the density of the phases calculated from the XRD structural data at 1100 °C (b), and calculated linear expansion of the coating at 1100 °C (c).

The length change of the free-standing coating at 1100 °C was also measured by dilatometry. As shown in Fig. 4a, two samples (sample #1 and #2) were heated up to 1100 °C and kept at this temperature for 10 and 30 h, respectively. Both samples showed a crystallization shrinkage (~0.75 %) at ~1050 °C. At 1100 °C, no length change was detected in the samples within the first ~3 h. After 3 h, the samples started to show non-linear expansion as a result of the M→S phase transformation. The transformation was not completed after 10 h at 1100 °C but approximately 1.34 % net expansion was measured after 30 h dwell time. A third sample was measured during continuous heating from room temperature up to 1400 °C in the dilatometer (Fig. 4b). Similar to the sample #1 and #2, this sample exhibited the same degree of shrinkage at ~1050 °C and the net rapid expansion at ~1200 °C was also about 1.3 % in agreement with the total expansion measured at 1100 °C after 30 h.

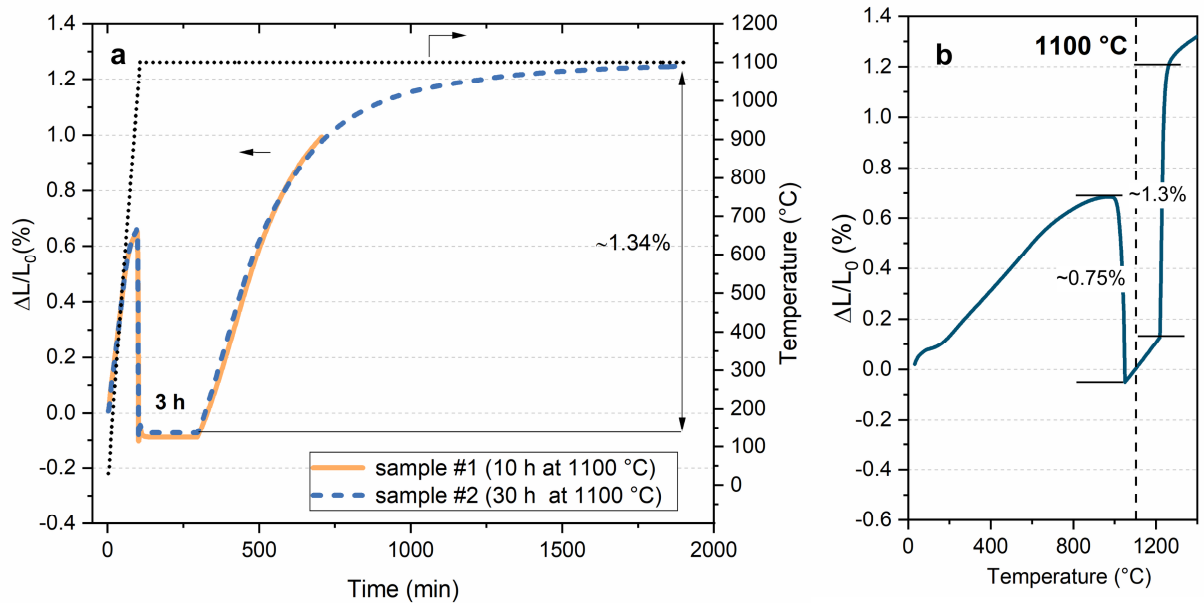

Fig. 4: Dilatometry measurement 1100 °C for 10 and 30 h (a), and during continuous heating between room temperature and 1400 °C (b).

Fig. 5a shows the comparison of calculated and measured expansions of the Yb-silicate coating using HT-XRD and dilatometry methods at 1100 °C. According to these results, the calculated net expansion in HT-XRD was ~35% larger than the measured expansion in dilatometry. Secondly, the onset of phase transformation and hence the resultant expansion was different in the two methods: the expansion promptly started at 1100 °C in HT-XRD measurements while it took 3 h in dilatometry. These discrepancies can be first attributed to differences in the measurement methods. In HT-XRD, only the surface of the Yb-silicate coating is analyzed within a depth of 20-30 µm while in dilatometry length change of the bulk with a thickness of ~2000 µm is recorded. In different silicate glass systems, faster crystal growth, as well as phase transformation kinetics at the free surfaces than in the bulk, were reported in the literature [28, 29]. Supporting this, room temperature XRD measurements at different depths (surface vs. after grinding halfway through the thickness of the sample) of a dilatometry sample after 0.5 h measurement at 1100 °C showed a higher degree of crystallinity at the surface (see supplementary data). Therefore it is plausible to assume that crystallization and phase transformation kinetics could be more sluggish in the dilatometry sample than at the sample surface analyzed by the XRD. This difference could explain some delay in the expansion at the beginning of the dilatometry measurement at 1100 °C. In HT-XRD, the sample is not constrained during the measurement while in the dilatometry a small contact force is applied to the sample by the push road which may have contributed to the lower expansion measured in the latter. Additionally, neglecting the amorphous content in the quantitative phase analysis introduced an error in expansion calculation at 1100 °C. Lastly, microstructural changes were observed in the sample at 1100 °C which would affect the measured expansion in the dilatometry method. Fig 5 b-d compares the microstructure of the free-standing coating in the as-sprayed state (b), after 0.5 h at 1100 °C (c) and after 30 h at 1100 °C (d). From these images, it was evident that the crack healing in the coating was progressing at the measurement temperature. Already after 0.5 h at 1100 °C, some crack healing was visible in the coating but particularly at the end of the measurement, the cracks were mainly transformed into a chain of pores as shown in the inset in Fig. 5d. This crack healing process may be limiting the expansion during the dilatometry measurements.

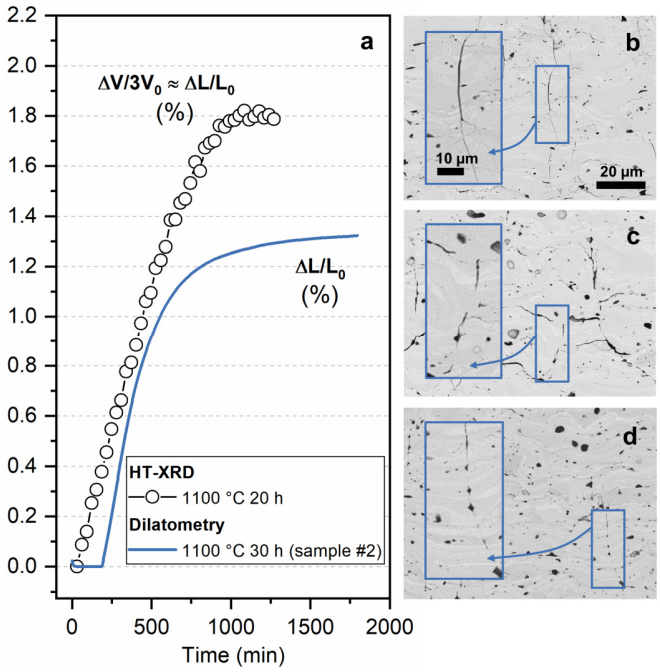

Fig. 5: Comparison of the calculated and measured expansions in the APS Yb-silicate coating by HT-XRD and dilatometry, respectively (a). The cross-section SEM microstructures of the free-standing coating in the as-sprayed state (b), after 0.5 h at 1100 °C (c) and after 30 h dilatometry measurement at 1100 °C (d). Note that the microstructural changes observed in the dilatometry samples were also found in HT-XRD samples.

The crack healing in the constrained Yb-silicate coatings (on Si/SiC) after heat treatment was reported earlier in the literature and the crack healing was attributed to the resultant volume expansion of M→S phase transformation in Yb-silicate [30]. The authors found a positive correlation between the expansion of the Yb-silicate coating detected by the dilatometry method and the degree of crack healing in the coating, i.e. the Yb-silicate coating sprayed at hotter conditions showed larger expansion as well as more pronounced crack healing [30]. Our findings however revealed that the coating does not need to be constrained on the substrate in order for crack healing to take place. Although this does not rule out the contribution of M→S transformation on crack healing in the constrained Yb-silicate coatings, it suggested an additional mechanism. We propose that viscous flow at the test temperature (up to 1100 °C) driven by the capillary forces in the partially amorphous free-standing coating may be responsible for crack spheroidization [31] and healing. After the crystallization was completed, which took ~7-8 h at 1100 °C, solid-state sintering may have also contributed to the densification of the free-standing coating microstructure.

To summarize, three different metastable phases, namely, $Yb_2Si_2O_7$ (M), Yb_2SiO_5 (M), and $Yb_{4.67}Si_3O_{13}$ (M), and two stable phases $Yb_2Si_2O_7$ (S), Yb_2SiO_5 (S) were found to be preferentially crystallizing from the amorphous Yb-silicate coating starting at 1000 °C. The metastable phases transformed to $Yb_2Si_2O_7$ (S), and Yb_2SiO_5 (S) at higher temperatures and the data presented in this work revealed that M→S phase transformation results in an expansion in the coating during the heat exposure. The transformation took about 30 h to be completed at 1100 °C in dilatometry measurements while it was rapid at ~1200 °C (~1 h). According to HT-XRD measurements, the transformation was completed in less than 20 h at 1100 °C, and the calculated net expansion was significantly larger (+35%) than the measured expansion in dilatometry. The difference in the estimated and measured expansions was attributed to different measurement volumes in the two

methods, assumptions made for the volume change calculation in HT-XRD as well as microstructural changes in the coating during measurements at 1100 °C. The microstructural investigations revealed crack healing in the coating which was associated with the lower expansion measured in dilatometry in comparison with the HT-XRD method. Viscous flow in the partially amorphous coating at the test temperature (up to 1100 °C) was proposed as the crack healing mechanism. This mechanism would rely on the initial amorphous content of the coating and only be active until the viscosity is raised by the crystallization. If this hypothesis is confirmed, it may have major implications for EBC processing as well as the design of post-process heat treatment.

Acknowledgments: The authors are grateful to Karl-Heinz Rauwald for thermal spray assistance and Marie-Theres Gerhards for conducting dilatometry measurements.

References:

[1] I. Spitsberg, J. Steibel, International Journal of Applied Ceramic Technology 1(4) (2004) 291-301.
[2] R. Naslain, F. Christin, MRS Bull. 28(9) (2011) 654-658.
[3] A. Chamberlain , J. Lane, SiC/SiC ceramic matrix composites: A turbine engine perspective, in: W. Fahrenholtz, W.E. Lee, E.J. Wuchina, Y. Zhou (Eds.) Proceedings of Ultra-High Temperature Ceramics: Materials For Extreme Environmental Applications II, Hernstein, Austria, 2012.
[4] N.P. Padture, Nat Mater 15(8) (2016) 804-809.
[5] K.N. Lee, D. Zhu, R.S. Lima, J. Therm. Spray Technol. (2021).
[6] K.N. Lee, Surf. Coat. Technol. 133–134 (2000) 1-7.
[7] H.E. Eaton, G.D. Linsey, K.L. More, J.B. Kimmel, J.R. Price, N. Miriyala, EBC Protection of SiC/SiC Composites in the Gas Turbine Combustion Environment, ASME Turbo Expo 2000: Power for Land, Sea, and Air, American Society of Mechanical Engineers, 2000, p. V004T02A018.
[8] K.N. Lee, D.S. Fox, N.P. Bansal, J. Eur. Ceram. Soc. 25(10) (2005) 1705-1715.
[9] J. Mesquita-Guimarães, E. García, P. Miranzo, M.I. Osendi, C.V. Cojocaru, R.S. Lima, Surf. Coat. Technol. 209 (2012) 103-109.
[10] K.N. Lee, Enviromental Barrier Coatings For SiC/SiC, in: N.P. Bansal, J. Lamon (Eds.) Ceramic Matrix Composites: Materials, Modeling and Technology, The American Ceramic Society, 2015.
[11] B.T. Richards, K.A. Young, F. de Francqueville, S. Sehr, M.R. Begley, H.N.G. Wadley, Acta Mater. 106 (2016) 1-14.
[12] E. Bakan, Y.J. Sohn, W. Kunz, H. Klemm, R. Vaßen, J. Eur. Ceram. Soc. 39(4) (2019) 1507-1513.
[13] K.N. Lee, J. Am. Ceram. Soc. 102(3) (2019) 1507-1521.
[14] B.E. Deal, A.S. Grove, J. Appl. Phys. 36(12) (1965) 3770-3778.
[15] E.J. Opila, J. Am. Ceram. Soc. 82(3) (1999) 625-636.
[16] R.C. Robinson, J.L. Smialek, J. Am. Ceram. Soc. 82(7) (1999) 1817-1825.
[17] E.J. Opila, J. Am. Ceram. Soc. 86(8) (2003) 1238-1248.
[18] E.J. Opila, J.L. Smialek, R.C. Robinson, D.S. Fox, N.S. Jacobson, J. Am. Ceram. Soc. 82(7) (1999) 1826-1834.
[19] E.J. Opila, D.S. Fox, N.S. Jacobson, J. Am. Ceram. Soc. 80(4) (1997) 1009-1012.
[20] M. Fritsch, H. Klemm, M. Herrmann, B. Schenk, J. Eur. Ceram. Soc. 26(16) (2006) 3557-3565.
[21] B.T. Richards, H.N.G. Wadley, J. Eur. Ceram. Soc. 34(12) (2014) 3069-3083.
[22] E. Bakan, D. Marcano, D. Zhou, Y.J. Sohn, G. Mauer, R. Vaßen, J. Therm. Spray Technol. 26(6) (2017) 1011-1024.

[23] E. Garcia, H.F. Garces, L.R. Turcer, H. Bale, N.P. Padture, S. Sampath, J. Eur. Ceram. Soc. 41(6) (2021) 3696-3705.
[24] H.M. Rietveld, Acta Cryst. 22(151-152) (1967).
[25] J. Felsche, J. Solid State Chem. 5(2) (1972) 266-275.
[26] P. Mechnich, Surf. Coat. Technol. 237 (2013) 88-94.
[27] A. Ito, J. Endo, T. Kimura, T. Goto, Mater. Chem. Phys. 125(1) (2011) 242-246.
[28] B.J. Harder, K.T. Faber, Scripta Mater. 62(5) (2010) 282-285.
[29] N. Diaz-Mora, E.D. Zanotto, R. Hergt, R. Müller, J. Non-Cryst. Solids 273(1) (2000) 81-93.
[30] E. Garcia, H. Lee, S. Sampath, J. Eur. Ceram. Soc. 39(4) (2019) 1477-1486.
[31] R. Girard, A. Faivre, F. Despetis, J. Am. Ceram. Soc. 97(11) (2014) 3463-3468.